**ORIGINAL ARTICLE**

**Journal Section**

# Robust Data-Driven Controller Design with Finite Frequency Samples

**Philippe Schuchert**[1] | **Alireza Karimi**[1]

[1]Laboratoire d'Automatique, EPFL, Lausanne, Switzerland

**Correspondence**
Prof. Alireza Karimi,
EPFL STI IGM SCI-STI-AK
ME C2 407 (Bâtiment ME)
Station 9
1015 Lausanne
Email: alireza.karimi@epfl.ch

**Funding information**
This work is funded by INNOSUISSE under grant no. *48289.1 IP-ENG* and the National Centres of Competence in Research under grant no. *565423 NCCR Automation*.

Modern control synthesis methods rely on accurate models to derive a performant controller. Obtaining a good model is often a costly step, and has led to a renewed interest in data-driven synthesis methods. Frequency-response-based synthesis methods have been proposed, as they rely on easy-to-obtain frequency-response data and offer flexible tuning approaches. Such methods formulate the objective as a minimization over the whole spectrum, which is problematic as only a finite number of frequency points can be considered when solving the problem using numerical solvers. Most methods require sampling the frequency response to obtain a trackable formulation, but this sampling process loses all stability and performance guarantees. By studying the inter-frequency behavior of such methods, bounds on the spectrum errors can be derived. Using these bounds, a novel algorithm is proposed to design a SISO controller using only a finite number of frequency response data, which guarantees closed-loop stability and robust performance.

**KEYWORDS**
Data-driven control, Robust control, optimization

**Abbreviations:** FRF, frequency response function.

# 1 | INTRODUCTION

Modern control synthesis methods rely on accurate models to derive an effective controller. Such models can sometimes be obtained using first principle modeling, but most cases require identifying a more suitable control-relevant model using input-output trajectories. In general, due to finite input/output data available, noisy measurements and structural mismatch, the process model cannot be exactly identified. Instead, only an estimate of the process model can be obtained, with associated error bounds. For example, the framework of identification in $\mathcal{H}_\infty$ aims to search for a model and corresponding uncertainty, see [1, 2, 3, 4]. These approaches typically result in a suitable model for the majority of practical applications, with asymptotic errors that bound the distance from the true process based on the length of the input/output data. Recently, newer data-driven methods have been developed to give probabilistic but non-asymptotic errors, e.g., [5, 6, 7] or [8] for a survey. In both cases, quantifying the modeling uncertainty is of great importance for control design. It should be incorporated in the control design phase, to guarantee performance for not only the estimated model but also the true underlying process. Model uncertainty can be elegantly described in the frequency domain [9], and therefore is well suited to be used in combination with frequency domain methods, such as $\mathcal{H}_\infty$ control. Recently, data-driven synthesis methods using the frequency-response function (FRF) have found renewed interest in data-driven methods. With the advent of more readily available computational power that can be used to automatically tune the controller parameters, multiple FRF-based data-driven synthesis methods have been proposed, e.g., [10, 11, 12, 13, 14, 15]. In these methods, the problem is formulated as an optimization problem over the whole frequency range, but to obtain a tractable formulation, it is proposed to sample the frequency spectrum. This sampling step results in losing all stability and performance certificates. Without careful supervision and possibly the intervention of an expert, such methods may result in controllers not stabilizing the closed loop. Additionally, most formulations are not designed to handle model uncertainty directly and require additional effort to guarantee robust performance. Both problems can be argued as very problematic and major drawbacks of such methods. The evaluation of stability (and performance) can only occur after tuning and may necessitate restarting with a denser frequency grid if the tuning procedure proves unsuccessful. Additional certificates should be computed on top of the synthesis procedure for these reasons, for example, as is done in [16].

This paper proposes a synthesis problem that is robust w.r.t. frequency sampling and model uncertainty, guaranteeing performance and robustness. This is achieved by studying the inter-frequency behavior in the SISO case of the method proposed in [17]. An iterative algorithm is developed which guarantees that the stage cost upper-bounds the true $\mathcal{H}_2$ or $\mathcal{H}_\infty$ closed loop norm, even when considering a finite number of frequencies and additive uncertainty for the process model. This is achieved by first finding sets that encapsulate the true frequency responses and then constraining these sets to ensure performance and robustness. Furthermore, we show that the proposed formulation is equivalent to [17] in the limit when the whole spectrum is considered.

This paper is organized as follows: in Sec. 2 preliminaries and a short overview of [17] is provided. In Sec. 3, developments for the proposed synthesis approach are presented, and the main results are discussed in Sec. 4. Finally, illustrative examples are given in Sec. 5. Developments and discussions are given for a discrete-time controller, but extension to continuous time is straightforward.

*Notations:* The Hermitian transpose of a matrix $F$ is denoted $F^*$. The element-wise absolute value of a vector $F$ is denoted $|F|$. The set of stable transfer functions bounded on the unit circle is denoted $\mathcal{RH}_\infty$. If $H$ is a discrete- or continuous-time transfer-function, then $H(j\omega)$ denotes its FRF at frequency $\omega$. To keep the notations short, the subscript $k$ will be used to denote a quantity related to $j\omega_k$, e.g., $H_k = H(j\omega_k)$. The (complex-valued) unit uncertainty ball is denoted $\Delta$, with $|\Delta| \leq 1$.

# 2 | PRELIMINARIES

## 2.1 | Problem description

To control a system, a mathematical representation is first required. It has been noted that first principle models often describe an idealized version of the system and fail to capture the intricacies encountered in a real process $\mathcal{P}$, and various methods have been proposed to address this issue. For example, in an idealized setup, the frequency response function (FRF) can be obtained everywhere and exactly using data-driven approaches, such as [18] which uses the Behavioral framework to derive the FRF.

In practice, various sources of errors do not allow exact identification of the process model, and an identification error is present. For example, this could be due to noise corrupting the measurements and finiteness of the data. It is therefore important to also account for these sources of errors when designing a controller regulating a process. The field of identification for control has brought forward various methods to obtain a control-relevant model $\hat{P}$. An estimate for the process's spectrum can then be obtained, for example, using Fourier analysis [19] when using a signal with bounded 2-norm:

$$\hat{P}(j\omega) = \left[\sum_{k=0}^{N-1} y(k)e^{-j\omega T_s k}\right]\left[\sum_{k=0}^{N-1} u(k)e^{-j\omega T_s k}\right]^{-1} \tag{1}$$

where $N$ is the number of data points, $T_s$ is the sampling period, and $u(k)$ and $y(k)$ represents respectively the inputs and the outputs at sample $k$.

Various examples are discussed in [20] to find the identification errors for the asymptotic regime case, and also highlights that such errors are best described in the frequency domain. In this paper, it is assumed that the identification errors can be expressed as

$$\sup_{\omega\in\Omega} |\hat{P}(j\omega) - \mathcal{P}(j\omega)| \leq \alpha(\rho, d, N). \tag{2}$$

Here, $\Omega = (-\pi/T_s, \pi/T_s]$ represents the frequency spectrum and $\alpha(\rho, d, N)$ is a function of intrinsic information of the system. Specifically, $\rho$ is the spectral norm of the state-transition matrix, $d$ signifies information regarding the process noise, and $N$ denotes the length of the data. Recent renewed interest has been found in finite data identification in the non-asymptotic regime. For example, [5] shows how to construct inputs $u(k)$ such that $\alpha$ in (2) is bounded. The estimated model and uncertainty might not always be specified exactly as in (2), but can often be converted to this form. In case the Hankel matrix of the system is first computed, one can also upper bound the $\mathcal{H}_\infty$ error between the true system and the computed approximation [21].

## 2.2 | Related work

Recent $\mathcal{H}_2$ and $\mathcal{H}_\infty$ data-driven control synthesis approaches [12, 13, 17] use an inner-approximation of the synthesis criterion to design a controller using only the FRF of a system, not requiring a parametric (e.g., state-space) model. We will give a summary of [17], which extends [12, 13], and serves as a departure point for the method presented in this paper.

A generalized LTI SISO system, mapping exogenous input $w \in \mathbb{R}$ and control input $u \in \mathbb{R}$ to performance channels

$z \in \mathbb{R}^{n_z}$ and measurements $y \in \mathbb{R}$ is given by:

$$\begin{aligned} z &= G_{11} w + G_{12} u, \\ y &= G_{21} w + G_{22} u. \end{aligned} \tag{3}$$

It is assumed that only the FRF of the generalized system

$$G(j\omega) = \left[\begin{array}{c:c} G_{11}(j\omega) & G_{12}(j\omega) \\ \hdashline G_{21}(j\omega) & G_{22}(j\omega) \end{array}\right] \tag{4}$$

is available, where $G_{ij}(j\omega)$ are FRFs of appropriate size. For simplicity, it is assumed that $G$ has no poles on the unit circle. The controller is parametrized as $K = X/Y$, where $X$ and $Y$ are both $\mathcal{RH}_\infty$ transfer functions. The synthesis objective is to design an LTI control law $u = Ky$, regulating the effect of the exogenous disturbances $w$ onto the performance channels $z$. The closed-loop (using positive feedback) system is given by

$$T_{zw} = G_{11} + G_{12} K (1 - G_{22} K)^{-1} G_{21}. \tag{5}$$

Several significant simplifications are made in comparison to [17], as $X, Y$, and $G_{22}$ are treated as scalar transfer functions. Moreover, $G_{21} = 1$, is chosen to greatly simplify the derivations. Then, the closed-loop can be expressed as

$$T_{zw} = G_{11} + G_{12} X (Y - G_{22} X)^{-1} = \left(G_{11}(Y - G_{22} X) + G_{12} X\right) / (Y - G_{22} X) \tag{6}$$

which can be rewritten concisely as $T_{zw} = (VY + WX)/\Phi$ where

$$V = G_{11} \tag{7}$$

$$W = G_{12} - G_{11} G_{22} \tag{8}$$

$$\Phi = Y - G_{22} X \tag{9}$$

The LFT framework uses the convention of positive feedback and corresponds to use $G_{22} = -\mathcal{P}$. Under the assumption that the closed-loop system is stable, the norms of $T_{zw}$ can be expressed using only its FRF:

$$\|T_{zw}\|_2^2 = \frac{T_s}{2\pi} \int_\Omega H(j\omega) d\omega =: J_2(H) \tag{10a}$$

$$\|T_{zw}\|_\infty^2 = \sup_{\omega \in \Omega} H(j\omega) =: J_\infty(H) \tag{10b}$$

where $H(j\omega) := T_{zw}^*(j\omega) T_{zw}(j\omega)$. Introducing an upper-bound $\gamma(j\omega)$ on $H(j\omega)$:

$$T_{zw}^*(j\omega) T_{zw}(j\omega) \leq \gamma(j\omega),$$

it can be shown that minimizing the $\mathcal{H}_2$ or $\mathcal{H}_\infty$ norm is equivalent to minimizing [17]

$$\min \; J_p(\gamma) \tag{11a}$$

subject to

$$\|VY + WX\|^2 \leq \gamma \Phi^* \Phi \quad \forall \omega \in \Omega \tag{11b}$$

$$X/Y \text{ stabilizes the closed-loop} \tag{11c}$$

This is a non-linear optimization problem, and the authors of [17] propose to find an inner approximation by substituting $\Phi^*\Phi$ by a (linear in optimization variables) lower bound $\Upsilon$:

$$\Upsilon \leq \Phi^* \Phi,$$

which is chosen in this case as

$$\Upsilon(\Phi, \Phi_c) = \Phi^*\Phi_c + \Phi_c^*\Phi - \Phi_c^*\Phi_c = 2\Re\{\Phi\Phi_c^*\} - |\Phi_c|^2. \tag{12}$$

With an appropriate choice of $\Phi_c$ it is shown in [17] that a sufficient condition for stability is $\Upsilon \geq 0$. The minimization problem can therefore be formulated as

$$\min \; J_p(\gamma) \tag{13a}$$

subject to

$$\|VY + WX\|^2 \leq \gamma \cdot \Upsilon \quad \forall \omega \in \Omega \tag{13b}$$

$$\Upsilon \geq 0 \quad \forall \omega \in \Omega \tag{13c}$$

Remark that (13) is a convex optimization problem, but is semi-infinite ($\forall \omega \in \Omega$) and cannot be solved using numerical solvers. The authors propose to solve the problem at only a finite number of frequencies $\{\omega_1, \ldots, \omega_{n_f}\}$ to obtain a tractable solution. When carefully selecting a dense grid, the solution of the sampled problem closely approximates the semi-infinite problem, but no guarantees of robustness or performance can be given. This is illustrated by the example from Sec. 5.2, when considering a reasonable frequency grid, the resulting controller after optimizing can fail to stabilize the closed loop.

The main contribution of this paper is the derivation of a variation of the formulation proposed in [17], which guarantees robustness and performance, even in the case where only a finite number of frequencies can be considered in the numerical optimizer.

## 3 | DEVELOPMENTS

### 3.1 | Signposting

We will use as a starting point the formulation proposed in [17] using the SOCP embedding given in (13). Since this problem can only be solved at a finite number of frequencies and $\mathcal{P}$ is unknown, additional care is required. Focusing

on the frequency interval

$$\Omega_k = [\omega_k, \omega_{k+1}]$$

where $\omega_{k+1} > \omega_k$, assume that we are given $\mathrm{u}_k$ such that

$$\|VY + WX\| \leq \mathrm{u}_k \quad \forall \omega \in \Omega_k,$$

and $\ell_k$ such that $\Upsilon$ can be lower-bounded by

$$0 \leq \ell_k \leq \Upsilon \quad \forall \omega \in \Omega_k,$$

then $\sigma_k$ that satisfies the following constraint

$$\|VY + WX\|^2 \leq \mathrm{u}_k^2 \leq \sigma_k \ell_k \leq \sigma_k \cdot \Upsilon$$

is an upper bound on $H(j\omega)$, i.e, $H(j\omega) \leq \sigma_k$. This value can be considered as the "local" $\mathcal{H}_\infty$ bound over the frequency interval $\Omega_k$. If $\sigma_k$ is obtained for each frequency interval and the frequency intervals cover the whole spectrum, i.e., $\omega_1 = -\pi/T_s$, $\omega_{n_f} = \pi/T_s$ and, this can be used to derive upper bounds on the system norm $T_{zw}$: For the $\mathcal{H}_\infty$ case

$$\tilde{J}_\infty(\sigma_k) := \max_k \sigma_k \geq \|T_{zw}\|_\infty^2. \tag{14}$$

and for the $\mathcal{H}_2$ case:

$$\tilde{J}_2(\sigma_k) := \frac{T_s}{2\pi} \sum_{k=0}^{n_f-1} (\omega_{k+1} - \omega_k)\sigma_k \geq \|T_{zw}\|_2^2, \tag{15}$$

since

$$(\omega_{k+1} - \omega_k)\sigma_k \geq \int_{\omega_k}^{\omega_{k+1}} \sup_{\omega \in \Omega_k} H(j\omega)\, d\omega \geq \int_{\omega_k}^{\omega_{k+1}} H(j\omega)\, d\omega. \tag{16}$$

The focus is therefore on deriving the lower and upper bounds, $\ell_k, \mathrm{u}_k$, as well as the choice of $\Phi_c$ in $\Upsilon$ to guarantee the stability of the closed loop.

## 3.2 | Linear interpolations

Since the behavior of the FRF can be arbitrarily complex (as long as continuous) between two consecutive frequency points, a simpler description is required first. The frequencies are restricted to the interval $\Omega_k$ in this section for conciseness. Given $\hat{P}_k$ and $\hat{P}_{k+1}$, define the interpolated model $\overline{P}$ as

$$\overline{P}(\lambda) = (1 - \lambda)\, \hat{P}_k + \lambda\, \hat{P}_{k+1},$$

where the linear interpolant $\lambda$ is defined as

$$\lambda(\omega) = \frac{\omega - \omega_{k+1}}{\omega_{k+1} - \omega_k} \in [0, 1].$$

Additionally, define the interpolation error $\beta$ as

$$\beta = \sup_{\omega \in \Omega_k} |\hat{P}(j\omega) - \overline{P}(\lambda)|. \tag{17}$$

which can be computed numerically by evaluating (17) on a dense frequency grid, since $\hat{P}(j\omega)$ is available $\forall \omega$. In case it is not possible to obtain $\hat{P}(j\omega)$ at all frequencies, which is, for example, the case when a periodic input signal is used and $\hat{P}(j\omega)$ is only available at a finite number of frequencies, bounds on the interpolation error can be obtained using only information of an exponential envelope bounding the impulse response, see [22]. Dependency of $\lambda$ on $\omega$ will be hereafter omitted. Using the triangle inequality, we have

$$|\overline{P} - \mathcal{P}| \leq \underbrace{|\overline{P} - \hat{P}|}_{=\text{interpolation error}} + \underbrace{|\hat{P} - \mathcal{P}|}_{=\text{identification error}} \leq \beta + \alpha. \tag{18}$$

for all $\omega \in \Omega_k$.

The maximum error $\delta_{\hat{P}} = \beta + \alpha$ from the interpolated model can be used to construct a set $\mathscr{P}$ that is guaranteed to contain the true process model $\mathcal{P}$:

$$\mathcal{P}(j\omega) \subseteq \overline{P}(\lambda) + \Delta\delta_{\hat{P}}. \tag{19}$$

**Remark** If an identification procedure is used which does not give $\alpha$, or an estimate thereof, one can always use $\alpha = 0$ to guarantee only stability of the nominal model $\hat{P}$.

Similarly, we are interested in quantifying the interpolation error of $V, W$. The main difference is that $V, W$ are vector-valued functions. Define $\delta_V, \delta_W$ as the interpolation errors of the weights used in the synthesis problem:

$$V(j\omega) \subseteq \overline{V}(\lambda) + \mathbf{\Delta}\delta_V, \tag{20}$$

$$W(j\omega) \subseteq \overline{W}(\lambda) + \mathbf{\Delta}\delta_W. \tag{21}$$

and the structured uncertainty ball as

$$\mathbf{\Delta} = \text{blkdiag}(\Delta, \ldots, \Delta) \in \mathbb{C}^{n_z \times n_z}.$$

Denoting $[T]_j$ the $j^{\text{th}}$ entry of a vector $T$, the interpolation errors are defined entry-wise as follows:

$$[\delta_V]_j = \sup_{\omega \in \Omega_k} |[V(j\omega)]_j - [\overline{V}(\lambda)]_j|,$$

and similarly for $\delta_W$. To compute the different errors, the simplest approach is to numerically compute the interpolation error by sampling the frequency responses on a dense grid (e.g., using $200 - 1000$ points between each pair of frequencies), and take the maximum among those points for the interpolation error.

Finally, define $\overline{X}(\lambda)$ and $\overline{Y}(\lambda)$ linear interpolations of the controller numerator $X$ and denominator $Y$. A similar construction can be done to overbound $X$ and $Y$:

$$X(j\omega) \subseteq \overline{X}(\lambda) + \Delta\delta_X, \tag{22}$$

$$Y(j\omega) \subseteq \overline{Y}(\lambda) + \Delta\delta_Y. \tag{23}$$

where $\delta_X \geq 0$, $\delta_Y \geq 0$ are bounds on the interpolation errors. For the controller, the numerator and denominator are not known in advance, and therefore, their interpolation errors cannot be evaluated in advance, but it is nevertheless desired to express these errors as a function of the controller parameters. Assume that $X$ and $Y$ are parametrized using a linear combination of proper rational transfer functions $R_m$ (e.g., Laguerre functions):

$$X = \sum_{m=0}^{M} x_m R_m(z), \quad Y = \sum_{m=0}^{M} y_m R_m(z) \tag{24}$$

where $x_m$, $y_m$ are real-valued optimization variables and $M$ is the order of the controller.

Then, the interpolation errors can be bounded using the triangle inequality

$$\left|X - \overline{X}(\lambda)\right| \leq \sum_{m=0}^{M} |x_m|\, \delta_{R_m} =: \delta_X, \tag{25a}$$

$$\left|Y - \overline{Y}(\lambda)\right| \leq \sum_{m=0}^{M} |y_m|\, \delta_{R_m} =: \delta_Y, \tag{25b}$$

where

$$\delta_{R_m} = \sup_{\omega \in \Omega_k} |R_m(j\omega) - \overline{R}_m(\lambda)|, \tag{26}$$

and $\delta_{R_m}$ can be obtained by evaluation on a dense grid. For conciseness, the dependence of $j\omega$ and $\lambda$ will be omitted when possible.

## 3.3 | Lower bounding $\Upsilon$

The focus of this section is initially finding a bound $\ell$ for $\Upsilon = 2\Re\{\Phi\Phi_c^*\} - |\Phi_c|^2$. By using the sets defined in the previous section and (9), it is straightforward to show that

$$\Phi \in \overline{Y} + \Delta\delta_Y + (\overline{P} + \Delta\delta_{\hat{P}})(\overline{X} + \Delta\delta_X). \tag{27}$$

Using the fact that

$$z \in \Delta(a + b\Delta) \implies z \in \Delta(|a| + |b|), \tag{28}$$

then (27) can be rewritten as

$$\Phi \in \overline{Y} + \overline{P}\,\overline{X} + \Delta(\delta_Y + |\overline{P}|\delta_X + |\overline{X}|\delta_{\hat{P}} + \delta_X\delta_{\hat{P}}). \tag{29}$$

With additional bounding using

$$|\overline{H}| \leq (1-\lambda)\,|H_k| + \lambda\,|H_{k+1}|$$

when $0 \leq \lambda \leq 1$, and appropriately factoring the different terms, a convex set $\mathscr{L}$ can be obtained such that $\Phi \in \mathscr{L}$:

**Lemma 1** *The set*

$$\mathscr{L} = Hull(p_0 + \Delta r_0, p_1 + \Delta r_1, p_2 + \Delta r_2) \tag{30}$$

*where $p_0, p_1, p_2$ are control points given by*

$$p_0 = Y_k + \hat{P}_k X_k, \tag{31a}$$
$$p_1 = 0.5(Y_k + Y_{k+1} + \hat{P}_k Y_{k+1} + \hat{P}_{k+1} Y_k), \tag{31b}$$
$$p_2 = Y_{k+1} + \hat{P}_{k+1} X_{k+1}, \tag{31c}$$

*and the associated radii $r_0, r_1, r_2$ given by*

$$r_0 = \delta_Y + \delta_X \delta_{\hat{P}} + \delta_X |\hat{P}_k| + \delta_{\hat{P}} |X_k|, \tag{32a}$$
$$r_1 = \delta_Y + \delta_X \delta_{\hat{P}} + 0.5\delta_X (|\hat{P}_k| + |\hat{P}_{k+1}|) + 0.5\delta_{\hat{P}} (|X_k| + |X_{k+1}|) \tag{32b}$$
$$r_2 = \delta_Y + \delta_X \delta_{\hat{P}} + \delta_X |\hat{P}_{k+1}| + \delta_{\hat{P}} |X_{k+1}|, \tag{32c}$$

*is a convex set such that $\Phi \in \mathscr{L}$.*

*Proof:* The proof is straightforward and is given in the Appendix.

The set $\mathscr{L}$ can be interpreted as bounding a Bézier curve [23]

$$B = (1-\lambda)^2 (p_0 + \Delta r_0) + 2(1-\lambda)\lambda (p_1 + \Delta r_1) + \lambda^2 (p_2 + \Delta r_2)$$

constructed in such way that $\Phi \in B$, with control disks $p_i + \Delta r_i$ instead of control points . An important property is that the convex hull of the control points bounds Bézier curves. This property also holds for this Bézier curve with control disks instead of control points:

$$B \subseteq \text{Hull}(p_0 + \Delta r_0, p_1 + \Delta r_1, p_2 + \Delta r_2). \tag{33}$$

Because any convex combination of the three control disks can be written as

$$\lambda_0 (p_0 + \Delta r_0) + \lambda_1 (p_1 + \Delta r_1) + \lambda_2 (p_2 + \Delta r_2)$$

for $\lambda_0$, $\lambda_1$, $\lambda_2 \geq 0$ and $\lambda_0 + \lambda_1 + \lambda_2 = 1$, and setting $\lambda_0 = (1-\lambda)^2$, $\lambda_1 = 2(1-\lambda)\lambda$, $\lambda_2 = \lambda^2$ results exactly in $B$.

Importantly, since $B$ is contained in the convex hull of the control disks, the point $p \in B$ with the lowest real part cannot be less than the lowest real part of the control disks $p_i + \Delta r_i$. A graphical illustration is given in Fig. 1 to highlight this fact. This can be used to find a lower bound $\ell_k$ of $\Upsilon = 2\Re\{\Phi\Phi_c^*\} - |\Phi_c|^2$ over the frequency range $\Omega_k$.

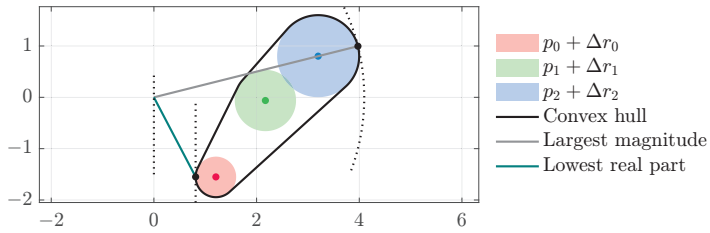


**FIGURE 1** Illustrative example of control disks and their convex hull. Additionally, the points with the lowest real part and with the largest magnitude are indicated using a black dot.

Since by construction $\Phi \in \mathscr{L}$, it is clear that if $\ell_k$ satisfies

$$\ell_k \leq \min_{|\Delta| \leq 1} 2\Re\{(p_i + \Delta r_i)\Phi_c^*\} - |\Phi_c|^2,$$

where $i \in \{1, 2, 3\}$, then this implies that $\ell_k \leq \Upsilon$. The worst case over all $|\Delta| \leq 1$ is given by $\Delta r_i \Phi_c = -r_i|\Phi_c|$ since $r_i \geq 0$, and therefore a lower bound of $\Upsilon$ can be formulated as

$$\ell_k \leq 2\Re\{p_0\Phi_c^*\} - 2r_0|\Phi_c| - |\Phi_c|^2, \tag{34a}$$

$$\ell_k \leq 2\Re\{p_1\Phi_c^*\} - 2r_1|\Phi_c| - |\Phi_c|^2, \tag{34b}$$

$$\ell_k \leq 2\Re\{p_2\Phi_c^*\} - 2r_2|\Phi_c| - |\Phi_c|^2. \tag{34c}$$

It should be noted that $r_i$ depends on the absolute values of the optimization variables. For example in (34a),

$$r_0 = \delta_Y + \delta_X \cdot (\delta_{\hat{P}} + |\hat{P}_k|) + \delta_{\hat{P}}|X_k| = \sum_{m=0}^{M} \delta_{R_m} \cdot \big((|y_m| + |x_m| \cdot (\delta_{\hat{P}} + |\hat{P}_k|)\big) + \delta_{\hat{P}}|X_k|.$$

using the definition of $\delta_X, \delta_Y$ given in (25), and therefore (34a) is not a linear inequality. Instead, (34a) can be implemented in a convex fashion, e.g., using the 1-norm cone [24]:

$$\| 2|\Phi_c| \; d_0 \|_1 \leq 2\Re\{p_0\Phi_c^*\} - |\Phi_c|^2 - \ell_k, \tag{35}$$

where $d_0 = [\delta_{\hat{P}}X_k, \; \delta_{R_0}y_0, \; a_m x_0, \; \ldots, \; \delta_{R_m}y_m, a_m x_m]^\top$ and $a_m = \delta_{R_m}(\delta_{\hat{P}} + |\hat{P}_k|)$. A similar construction can be obtained for (34b)–(34c). In practice, appropriate modeling languages for convex optimization, e.g., [25], recognize 34 as a conic constraint and do not require the transformation (35).

## 3.4 | Upper-boundding $VY + WX$

A similar approach will be used to construct an upper bound on $\|VY+WX\|$. A set $\mathscr{Q}$ can be constructed, guaranteeing that the vector $VY + WX$ is located inside:

$$VY + WX \in \mathscr{Q}.$$

The set

$$\mathscr{Q} = \mathrm{Hull}(q_0 + \mathbf{\Delta} s_0, q_1 + \mathbf{\Delta} s_1, q_2 + \mathbf{\Delta} s_2), \tag{36}$$

where the (vector-valued) control disk centers are given by

$$q_0 = V_k Y_k + W_k X_k, \tag{37a}$$
$$q_1 = 0.5(V_k Y_{k+1} + V_{k+1} Y_k + W_k X_{k+1} + W_{k+1} X_k), \tag{37b}$$
$$q_2 = V_{k+1} Y_{k+1} + W_{k+1} X_{k+1}, \tag{37c}$$

with their associated radii by

$$s_0 = \delta_V \delta_Y + \delta_V |Y_k| + \delta_Y |V_k| + \delta_W \delta_X + \delta_W |X_k| + \delta_X |W_k|, \tag{38a}$$
$$s_2 = \delta_V \delta_Y + \delta_V |Y_{k+1}| + \delta_Y |V_{k+1}| + \delta_W \delta_X + \delta_W |X_{k+1}| + \delta_X |W_{k+1}|, \tag{38b}$$
$$s_1 = 0.5 \cdot (s_0 + s_2). \tag{38c}$$

is a convex set such that $WY + WX \in \mathscr{Q}$. For conciseness, the derivation of $p_i, s_i$ are given in Appendix A as the derivation is similar to $\mathscr{L}$ given in Lemma 1.

The set $\mathscr{Q}$ is a convex combination of control disks $q_i + \mathbf{\Delta} s_i$, and the distance of the furthest point of $\mathscr{Q}$ from the origin must be achieved on the boundary of one of the control disks. This is equivalent to finding the smallest $\mathrm{u}_k$ such that

$$\| \, |q_0| + s_0 \, \| \leq \mathrm{u}_k \tag{39a}$$
$$\| \, |q_1| + s_1 \, \| \leq \mathrm{u}_k \tag{39b}$$
$$\| \, |q_2| + s_2 \, \| \leq \mathrm{u}_k \tag{39c}$$

holds since $|q_i + \mathbf{\Delta} s_i| \preceq |q_i| + s_i$ where $\preceq$ denotes the element-wise inequality. The constraints (39) is convex, but auxiliary variables $d_i$ are required to implement it using standard optimization cones [24]:

$$\| \, d_i \, \| \leq \mathrm{u}_k \tag{40a}$$
$$|q_i| + s_i \preceq d_i \tag{40b}$$

Similar to (34), appropriate convex modeling languages can be used to implement these constraints easily.

## 4 | MAIN RESULTS

### 4.1 | Computing $\Phi_c$

In (34), a condition on the lower bound is derived but requires a choice of $\Phi_c$. In this section, we will describe the recommended choice of $\Phi_c$, which will guarantee the stability of the closed-loop.

Given a stabilizing controller $K_c = X_c/Y_c$ where $X_c, Y_c \in \mathcal{RH}_\infty$ coprime, compute the sets

$$X_c(j\omega) \subseteq \overline{X}_c(\lambda) + \Delta\delta_{X_c}, \tag{41}$$

$$Y_c(j\omega) \subseteq \overline{Y}_c(\lambda) + \Delta\delta_{Y_c}. \tag{42}$$

where $\delta_{X_c}, \delta_{Y_c}$ are computed analogously to (25). Compute the set $\mathscr{L}_c$ and its associated control disks overbounding $Y_c + \mathcal{P}X_c$ in a similar fashion as was done for $\mathscr{L}$. If $0 \notin \mathscr{L}_c$, choose $\Phi_c$ as the point inside this convex hull closest to the origin:

$$\Phi_c = \arg\min_{p \in \mathscr{L}_c} |p|^2 \tag{43}$$

This choice is made as it guarantees a solution to the optimization problem proposed later in Algorithm 1 and can be used to show that this algorithm converges monotonically. The point $\Phi_c$ can be computed using basic geometry and does not require solving an optimization problem:

1. Compute the closest points $p$ to the origin of each control disk of $\mathscr{L}_c$,
2. Compute the segment tangent to the boundary of each pair of control disks and compute the closest points $p$ on each segment to the origin,
3. Among all those points, select the point $p$ closest to the origin, i.e., the point with the lowest magnitude.

If $0 \in \mathscr{L}_c$, this may indicate a severe undersampling of the frequency responses. This is the case in the example given in Sec. 5.2, where a very coarse frequency grid with only 20 frequency points is taken to describe the FRF of a system of order 10. Moreover, a resonance peak is not sampled at all, leading to a significant conservatism and ultimately to $0 \in \mathscr{L}_c$. Since the controller $K_c$ was assumed to be stabilizing and $X_c, Y_c$ coprime, then

$$0 \notin Y_c + (\hat{P} + \Delta\alpha) X_c,$$

as otherwise there would exist a $\Delta$ such that at least one of the sensitivity function

$$\mathcal{S} = \frac{Y_c}{Y_c + (\hat{P} + \Delta\alpha) X_c}, \; \mathcal{T} = \frac{(\hat{P} + \Delta\alpha) X_c}{Y_c + (\hat{P} + \Delta\alpha) X_c},$$

is not finite as the denominator is zero at some frequency but not the numerator since $X_c, Y_c$ are coprime and cannot be both zero simultaneously; therefore, the closed-loop is unstable. This contradicts the assumption that $K_c$ is stabilizing. In the limit $|\omega_{k+1} - \omega_k| \to 0$, the set $\mathscr{L}_c$ reduces to $\mathscr{L}_c = Y_c + (\hat{P} + \Delta\alpha) X_c$ as all interpolation errors vanish. It is always possible to increase the number of frequency points until $0 \notin \mathscr{L}_c$ holds. In general, it is recommended to have sufficient frequency points where the phase or magnitude of $P$ is rapidly changing and similarly when the magnitude of $V$ or $W$ rapidly changes.

## 4.2 | Proof of stability

Boundedness of the FRF does not imply stability, and therefore it is important to show that the presented synthesis approach, when using the choice of $\Phi_c$ presented in (43), also embeds a guarantee of closed-loop stability. This will

be achieved using the sets $\mathscr{L}$ and $\mathscr{L}_c$ derived in the previous section: since these sets are by construction guaranteed to contain $Y + \mathcal{P}X$ and $Y_c + \mathcal{P}X_c$ respectively, it will be shown that the winding number of $Y + \mathcal{P}X$ must be equal to the winding number of $Y_c + \mathcal{P}X_c$. Finally, stability can be deduced using a theorem given in [17].

The previous section focused only on the interval $\omega \in \Omega_k$. The different values $p_i, r_i, p_i, s_i, \mathscr{L}_c, \Phi_c$ must be computed for each frequency interval and will hereafter be denoted respectively $p_{ik}, r_{ik}, p_{ik}, s_{ik}, \mathscr{L}_{ck}, \Phi_{ck}$, to explicitly indicate their association with the frequency interval.

**Theorem 1** *Given a stabilizing controller $K_c = X_c/Y_c$ where $X_c, Y_c \in \mathcal{RH}_\infty$, the closed-loop system with the controller $K = X/Y$ where $X, Y \in \mathcal{RH}_\infty$ is also stable if for all $k \in \{1, 2, \ldots, n_f - 1\}$ there exists $\ell_k \geq 0$ such that* (34) *holds, with $\Phi_{ck} \neq 0$ as given in* (43)*.*

*Proof:* Using Theorem 1 presented in [17], it is sufficient to show that the FRF of $Y + \mathcal{P}X$ and $Y_c + \mathcal{P}X_c$ have the same winding number to prove that $K$ is stabilizing the closed-loop. To proceed, we propose to compute the phase difference between both FRFs. The difference in angle can be bounded for $\omega \in \Omega_k$ by

$$\begin{aligned} |\measuredangle\{(Y_c + \mathcal{P}X_c)^*(Y + \mathcal{P}X)\}| &= |\measuredangle\{(Y_c + \mathcal{P}X_c)^*\Phi_{ck}\Phi_{ck}^*(Y + \mathcal{P}X)\}| \\ &\leq |\measuredangle\{(Y_c + \mathcal{P}X_c)^*\Phi_{ck}\}| + |\measuredangle\{(Y + \mathcal{P}X)\Phi_{ck}^*\}| \end{aligned}$$

since multiplying a by a positive value $\Phi_{ck}\Phi_{ck}^*$ does not change the angle. If the (absolute value of the) phase difference is always less than $\pi$, this implies that both FRFs must have the same winding number (see Appendix B for a proof). This will be proved by showing that each term of the right hand side of the above inequality is less than $\pi/2$.

The set $\mathscr{L}$ , which can be described using the convex combination of $p_{ik} + \Delta r_{ik}$, $i = \{1, 2, 3\}$, satisfies by construction

$$Y + \mathcal{P}X \in \mathscr{L}$$

for $\omega \in \Omega_k$. If (34) holds with $\ell_k \geq 0$, then $\Upsilon \geq 0$ and

$$\Re\{(Y(j\omega) + \mathcal{P}(j\omega)X(j\omega))\Phi_{ck}^*\} \geq \frac{1}{2}|\Phi_{ck}|^2 > 0.$$

Therefore $|\measuredangle\{(Y + \mathcal{P}X)\Phi_{ck}^*\}| < \pi/2$, since any complex number with a strictly positive real part has an angle between $(-\frac{\pi}{2}, \frac{\pi}{2})$. Now it remains to choose $\Phi_{ck}$ such that $(Y_c + \mathcal{P}X_c)\Phi_{ck}^*$ has also strictly positive real part. If $\Phi_{ck} \neq 0$ is chosen as given in (43), then multiplying $(Y_c + \mathcal{P}X_c)$ by $\Phi_{ck}^*$, rotates (and scales) $\mathscr{L}_{ck}$ and its convex hull into the right-half plane as it is illustrated in Fig. 2. In particular, any point $z \in \mathscr{L}_{ck}$ will also have a positive real part after multiplication by $\Phi_{ck}^*$ and

$$\Re\{\Phi_{ck}^* z\} \geq \Re\{\Phi_{ck}^*\Phi_{ck}\} = |\Phi_{ck}|^2 > 0 \quad \forall z \in \mathscr{L}_{ck}.$$

as $\Phi_{ck}$ is chosen as the point in $\mathscr{L}_{ck}$ with the lowest magnitude. Since we have constructed the set $\mathscr{L}_{ck}$ such that $Y_c(j\omega) + \mathcal{P}(j\omega)X_c(j\omega) \in \mathscr{L}_{ck}$ holds, it is therefore also guaranteed that

$$\Re\{(Y_c(j\omega) + \mathcal{P}(j\omega)X_c(j\omega))\Phi_{ck}^*\} > 0$$

holds for all $\omega \in \Omega_k$ and $|\measuredangle\{(Y_c + \mathcal{P}X_c)^* \Phi_{ck}\}| < \pi/2$. Therefore, using Theorem 1 in [17], the controller $K = X/Y$ must also stabilize the closed loop. ■

**Remark** For a stable system, a possible choice is always $X_c = 0$ and $Y_c = 1$. It is reasonable to assume knowledge of such a stabilizing controller for unstable systems to collect input-output trajectories for identification.

## 4.3 | Iterative algorithm and Asymptotic behavior

Similar to [17], an inner approximation of the original problem around some $X_c, Y_c$ was performed to obtain a convex formulation. We propose employing an iterative scheme to converge to a local minimum, summarized in Algorithm 1.

**Data:** $\{\hat{P},\ \alpha,\ \{\omega_1, \ldots, \omega_{n_f}\},\ V,\ W,\ X_c,\ Y_c,\ \varepsilon\}$
Set $\tilde{J}_{\text{pred}} \leftarrow \infty$
**while** *true* **do**
1) Compute the control disks $p_{ik}, r_{ik}, p_{ik}, s_{ik}$ as a function of the controller parameters.
2) Compute $\Phi_{ck}$ for every frequency interval $\Omega_k$.
3) Solve the following convex optimization problem:

$$\min_{X,Y,\sigma_k,\ell_k,\mathrm{u}_k} \ \tilde{J}_p(\sigma_k)$$

subject to, for every frequency interval $\Omega_k$:

$$\mathrm{u}_k^2 \leq \sigma_k \ell_k,\ \ell_k \geq 0$$

$$\| \, |q_{ik}| + s_{ik} \, \| \leq \mathrm{u}_k \quad \forall i \in \{1,2,3\}$$

$$\ell_k \leq 2\Re\{p_{ik}\Phi_{ck}^*\} - 2r_{ik}|\Phi_{ck}| - |\Phi_{ck}|^2 \quad \forall i \in \{1,2,3\}$$

**if** $\tilde{J}_{\text{pred}} - \tilde{J}_p(\sigma_k) \leq \varepsilon$ **then**
return $K = X/Y, \tilde{J}_p(\sigma_k)$
**else**
4) Set $X_c \leftarrow X, Y_c \leftarrow Y, \tilde{J}_{\text{pred}} \leftarrow \tilde{J}_p(\sigma_k)$
**end**
**end**

**Algorithm 1:** Iterative algorithm returning a controller $K = X/Y$ with closed-loop performance at least $\tilde{J}_p(\sigma_k)$

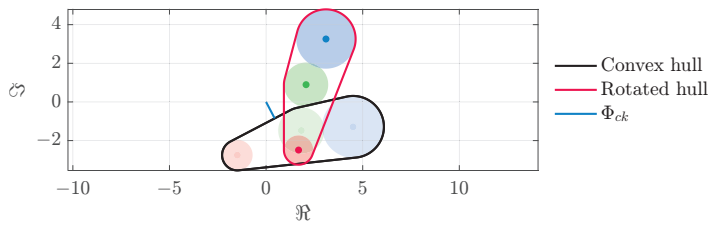


**FIGURE 2** Multiplying by $\Phi_c^*$, where $\Phi_c \neq 0$ is the closest point to the origin inside $\mathscr{L}_c$, rotates (and scales) the set into the right-half plane

With the choice of $\Phi_c$ presented in (43), $X = X_c, Y = Y_c$ is by construction a solution to the optimization problem in Algorithm 1. It should be noted that $X = X_c, Y = Y_c$ is always possible after iteration 1, due to step 4. Since the inner-approximation was chosen as $\Upsilon \leq \Phi^*\Phi$, we have

$$\ell_k \leq \min_{z \in \mathscr{L}_c} 2\Re\{z\Phi_c^*\} - |\Phi_c|^2 \leq \min_{z \in \mathscr{L}_c} |z|^2. \tag{45}$$

The $z$ minimizing the right-most hand-side of the equation in (45) is none else than the recommended $\Phi_c$ in (43) at the next iteration, as $\mathscr{L}$ corresponds to $\mathscr{L}_c$ of the next iteration due to step 4. Simple substitution shows that $\{X_c, Y_c, \sigma_k, \ell_k, \mathrm{u}_k\}$ is a possible solution to the optimization problem at the next iteration, and therefore the stage cost $\tilde{J}_p(\sigma_k)$ is not increasing. This means Algorithm 1 will converge monotonically.

This local minimum can be detected by computing the difference in stage cost $\tilde{J}_{\mathrm{pred}} - \tilde{J}_p(\sigma_k)$ between the current iteration and the last iteration. If this difference is smaller than a chosen value $\varepsilon$, e.g., around the numerical solver precision or user-defined tolerance, it is safe to assume that the algorithm converged to a local minimum or saddle point.

**Remark** Constraints will be automatically satisfied for frequencies $[-\omega_{k+1}, -\omega_k]$ if they are satisfied for $[\omega_k, \omega_{k+1}]$. It is therefore sufficient to consider only the half-spectrum, corresponding to $\omega_1 = 0$, $\omega_{n_f} = \pi/T_s$

**Remark** Different steps have been taken to over-bound the behavior between two consecutive frequencies. When the spectrum is sampled densely, i.e., $\lim |\omega_{k+1} - \omega_k| \to 0 \; \forall k$ (and $\alpha \to 0$), it is straightforward to show that the original formulation (13) is retrieved: $p_0 = p_1 = p_2 = \Phi$, $q_0 = q_1 = q_2 = VY + WX$ and the interpolations errors $s_i = 0$, $r_i = 0$. In this case, $\Phi_c$ also corresponds to the choice proposed in [17]. Simple back-substitution results in $\|VY + WX\|^2 \leq \gamma Y$, $\Upsilon \geq 0$, which is none other than the original problem considering the whole frequency spectrum.

**Remark** One can naturally increase the number of frequency points to reduce the conservatism introduced by over-bounding the various sets. Asymptotically, doubling the number of frequency points reduces by a factor of four the magnitude of the errors $r_i, s_i$. The optimization problem is formulated as a SOCP, and can be solved very efficiently, even for a large number of frequencies.

**Remark** It is shown in [26] that sufficiently increasing the controller order $M$ will result in a controller arbitrarily close to the global optimum of (11). This is also the case for Alg. 1, as long as the frequency spectrum is sampled sufficiently densely.

## 5 | NUMERICAL EXAMPLES

Three examples are used to demonstrate the usefulness of the proposed approach. First, a practical example is given using a real servomechanism. The second example showcases a situation where [17] fails even when considering a reasonable number of frequencies, but the proposed method still yields a performant controller. Despite employing several (over-)bounding steps, the final example illustrates that the suggested approach outperformed a comparable method.

### 5.1 | Servomechanism example

The proposed approach is demonstrated in a real experimental setup. The setup consists of a Servomechanism, where torque can be applied using a DC motor. A pseudo-random binary signal is applied to the system's input and 10 periods

each of length $N = 991$ are recorded. The signal is generated using a quadratic residue code, see [19]. The input-output dataset is split into 10 different sets. Part of the input-output data is shown in Fig. 3.

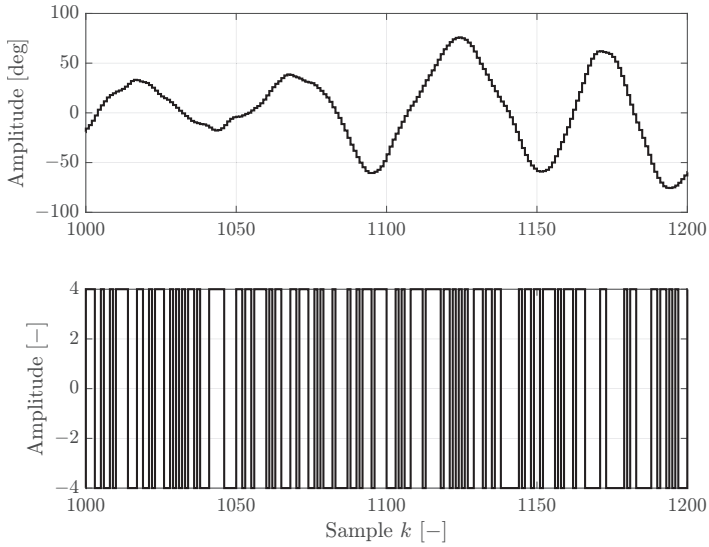


**FIGURE 3** Excerpt input-output experimental data.

For each period $p$, the FRF $\hat{P}_i(j\omega_k)$ can be computed at frequencies $\omega_k = 2\pi k/N, k = 0, \ldots, N-1$ using the FFT algorithm. The model $G$ is then computed as

$$P(j\omega_k) = \mathbb{E}[\hat{P}_i(j\omega_k)],$$

where $\mathbb{E}$ the expected value, and associated variance

$$\mathrm{Var}[P(j\omega_k)] = \mathbb{E}\left[\left(\hat{P}_i(j\omega_k) - \mathbb{E}[\hat{P}_i(j\omega_k)]\right)^2\right].$$

To be on the safe side, the identification error $\alpha = \alpha(j\omega_k)$ for the interval $\omega_k \leq \omega < \omega_{k+1}$ is taken as three times standard deviation:

$$\alpha(j\omega) = 3 \cdot \max\left\{\sqrt{\mathrm{Var}[\hat{P}(j\omega_k)]}, \sqrt{\mathrm{Var}[\hat{P}(j\omega_{k+1})]}\right\}$$

Since periodic data is used as input, information of $\hat{P}(e^{j\omega})$ outside frequencies $\omega_k$ is not available. Nevertheless, given the impulse response $g$ of $\mathcal{P}$ such that

$$|g_k| \leq C\rho^k, \quad k \geq 0,$$

it is shown in [22] that the error between the linearly interpolated frequency response and the underlying process is

bounded by

$$\beta \leq \frac{1}{2}\frac{C\rho(\rho+1)}{(1-\rho)^3}\left(\frac{\omega_{k+1}-\omega_k}{2T_s}\right)^2.$$

Applying an impulse directly to the system's input and measuring the output for obtaining the impulse response is a potential approach. However, this can result in saturation and should be avoided. Instead, we propose to apply a step-reference signal to the system and record the output $y$. An estimate for the impulse response $g_k$ is then given by

$$g_k = (y_k - y_{k-1})/d,$$

where $d$ is the amplitude of the step reference. An exponential envelope for the impulse response can be derived and is illustrated in Fig. 4. The coefficients $C = 4.413, \rho = 0.980$ are obtained by minimizing the following optimization

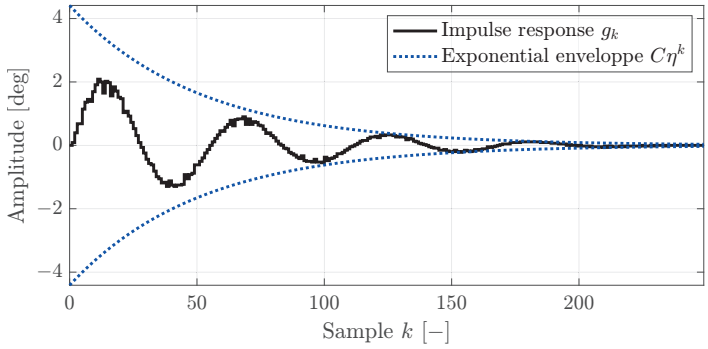


**FIGURE 4** Best fit of envelope bounding the impulse response.

problem:

$$\begin{aligned}
&\underset{C,\rho}{\arg\min}\ C\rho(\rho+1)/(1-\rho)^3\\
&\text{subject to:}\\
&|g_k| \leq C\rho^k \quad \forall k \geq 0\\
&C \geq 0,\ 0 \leq \rho < 1.
\end{aligned}$$

The design objective is to minimize the two-norm of

$$T_{zw} = \left\| \begin{bmatrix} 1/(z-0.9)\cdot\mathcal{S} \\ 5\cdot\mathcal{U} \end{bmatrix} \right\|_2,$$

and corresponds to the generalized system

$$G(j\omega) = \left[\begin{array}{c|c} 1/(z-0.9) & -\mathcal{P}/(z-0.9) \\ 0 & 5 \\ \hdashline 1 & -\mathcal{P} \end{array}\right].$$

The associated vectors $V, W$ are

$$V = \begin{bmatrix} 1/(z-0.9) \\ 0 \end{bmatrix}, W = \begin{bmatrix} 0 \\ 5 \end{bmatrix}.$$

A controller $K = X/Y$ parametrized using the pulse basis $R_m = z^{-m}$:

$$X = \sum_{m=0}^{M} x_m z^{-m}, Y = \sum_{m=0}^{M} x_m z^{-m}$$

is used to close the loop. To ensure zero steady-state error for a step signal, an integrator is added to the controller by adding a constraint $Y(z=1) = 0$ to the optimization problem. The order of the controller is taken as $M = 10$, and, since the system is open-loop stable, $X_c = 0, Y_c = 1$ is used.

The problem is solved at the frequencies obtained from the FFT. Closed-loop tracking performance is shown in Fig. 5, where the reference is a square waveform, along with the closed-loop response resulting from the synthesis method proposed in [17] only considering the nominal model $\hat{P}$.

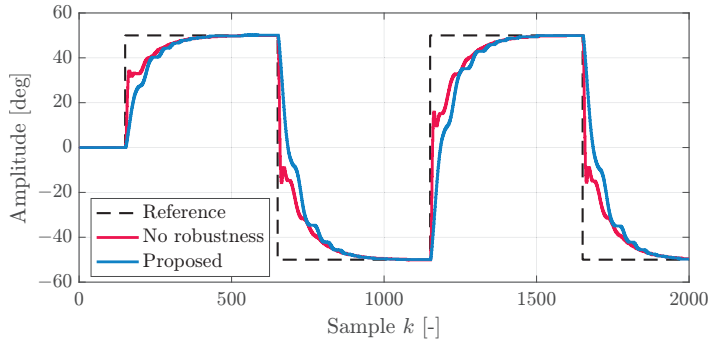


**FIGURE 5** Tracking of a square waveform on the actual system.

## 5.2 | Parametric example

In the previous example, the closed loop using the formulation proposed in [17] results in a stable closed loop. To illustrate the benefits over the original formulation, a system $\hat{P}$ whose frequency response is shown in Fig. 6 is taken as an example, which has one unstable pole, and associated uncertainty $\alpha = 0.25$. For reproducibility, the poles $p$

zeros $z$ and gain $g$ of this transfer function are listed below:

$$z = [0.12 + 1.05j,\ 0.12 - 1.05j,\ 0.81,\ 0.33,\ -0.94 + 0.45j,\ -0.94 - 0.45j,\ -0.32 + 0.04j,\ -0.32 - 0.04j,\ -0.88,\ -0.8]$$
$$p = [0.08 + 0.850j,\ 0.08 - 0.85j,\ 0.61,\ 0.4,\ -0.79 + 0.49j,\ -0.79 - 0.49j,\ -0.30,\ -0.4,\ -0.84,\ -0.82,\ 1.4],\ g = 1$$

Possible realizations of the transfer function for $\mathcal{P} = \hat{P} + \alpha\Delta$, where $\Delta$ here represents a stable system with $\|\Delta\|_\infty \leq 1$, are also shown in Fig. 6. The frequency grid is chosen as $n_f$ linearly spaced points between 0 and $\pi$ ($T_s = 1$).

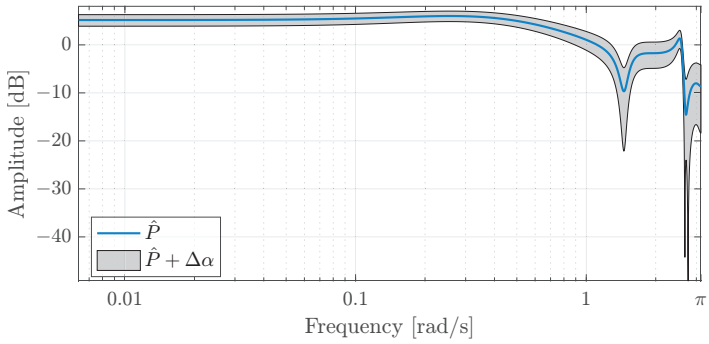


**FIGURE 6** Magnitude response of nominal model $\hat{P}$ and possible values of $\mathcal{P} \in \hat{P} + \Delta\alpha$.

Since the system is open-loop unstable, an initial controller is required. This controller is chosen as $X_c = 0.75$, $Y_c = 1$.

The synthesis objective is to minimize the closed-loop norm with $V = 0.1/(z - 0.9)^3$, $W = 0$. It should be noted that this example is chosen to highlight situations where [17] performs particularly poorly. Only the sensitivity $\mathcal{S}$ is minimized, and the weighing filter $V$ has a large magnitude at low frequencies.

Since the system has one unstable pole, due to the waterbed effect, the sensitivity $\mathcal{S}$ will have a large magnitude at high frequencies, in this case, peaks around 40dB, resulting in instability when the inter-frequency behavior is not accounted for. First, a comparison is made when only using the nominal model, that is, $\alpha = 0$ since [17] cannot directly handle robust performance. The stability of the closed-loop after tuning is reported in Table 1 using a varying number of frequencies and the controller order $M = 4$. In Table 1, one additional frequency point is added to the frequency set for $n_f = 20$ to satisfy $0 \notin \text{Hull}(\mathscr{L}_c)$.

**TABLE 1** Closed-loop stability with $M = 4$ after tuning using a different number of frequency points, with $\alpha = 0$. S = stable, U = unstable

| $n_f$ | 20(+1) | 50 | 100 | 250 | 500 | 1000 |
|---|---|---|---|---|---|---|
| Proposed | S | S | S | S | S | S |
| [17] | U | U | U | U | U | S |

The convex optimization problem in Alg. 1 is solved using the numerical solver *Clarabel* [27]. As can be observed, a significant advantage is that stability is guaranteed regardless of the number of frequencies.

Using the same example, we show that conservatism due to the different steps vanishes quickly. Synthesis performance with controller order $M = 10$ and $\alpha = 0.25$ is reported in Table 2. To compute the norm of the closed-loop, 200 realizations of $\Delta$ are taken, and $\|T_{zw}\|_\infty$ corresponds to the worst-case $\mathcal{H}_\infty$ norm. As can be seen, the value of

$\tilde{J}_\infty(\sigma_k)$ is always higher than the worst-case norm and correctly serves as a certificate for robust performance. The proposed method is solved for increasing numbers of frequency points $n_f$

**TABLE 2** Closed-loop stability with controller order $M = 10$ after tuning using a different number of frequency points, with $\alpha = 0.25$.

| $n_f$ | 20(+1) | 50 | 100 | 250 | 500 | 1000 |
|---|---|---|---|---|---|---|
| $\sqrt{\tilde{J}_\infty(\sigma_k)}$ | 24.55 | 2.656 | 1.435 | 1.166 | 1.117 | 1.095 |
| $\|T_{zw}\|_\infty$ | 3.834 | 1.923 | 1.273 | 1.132 | 1.105 | 1.092 |

The closed-loop singular values for $T_{zw} = V/(1 + (\hat{P} + \Delta\alpha)K)$ are shown in Fig. 7. As can be seen, the computed upper bound is above all possible realizations of $T_{zw}$.

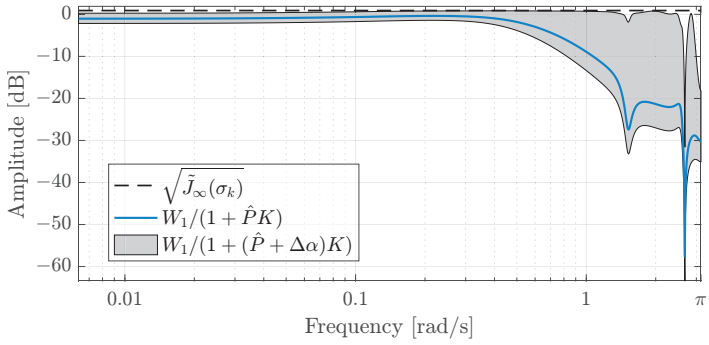


**FIGURE 7** Singular value of the closed-loop

## 5.3 | Conservatism due to overbounding

To showcase that, even though multiple overbounding steps have been taken, the conservatism introduced is small compared to other approaches, the proposed method is compared to [28] using their proposed example. The objective is to match the open loop to a reference loop $L_d$, and is formulated as minimizing

$$\sum_{k=1}^{n_f} \left|\hat{P}(j\omega_k)K(x, j\omega_k) - L_d(j\omega_k)\right|^2, \tag{46}$$

where $K(x, z) = x_0 + x_1 z^{-1}$ using $n_f$ linearly spaced frequencies $\omega_k$ between 0 and the Nyquist frequency. Additionally, a modulus margin of $M_m = 0.5$ must be guaranteed.

In [28], only the numerator can be tuned. For the sake of comparison, this choice is also made here and achieved using

$$X = x_1 + x_2 z^{-1}, \; Y = 1.$$

In this case, the modeling error is not considered ($\alpha = 0$), and the interpolation errors $\beta$ are computed numerically.

The modulus margin condition is equivalent to

$$\|M_m \mathcal{S}\|_\infty \leq 1,$$

where $\mathcal{S}$ the closed-loop sensitivity, and can be enforced using the proposed formulation by adding a constraint $\tilde{J}_\infty(\sigma_k) \leq 1$ and using $V = 1$, $W = 0$ in the optimization problem. The objective (46) is minimized, instead of $\tilde{J}_\infty(\sigma_k)$. This problem is solved for increasing values of $n_f$, and results are reported in Tab. 3. As can be seen, the proposed formulation can handle a much lower number of frequency points without adding significant conservatism.

**TABLE 3** Controller parameters obtained after tuning

| | [28] With guarantees | | [28] No guarantees | | Proposed | |
|---|---|---|---|---|---|---|
| $n_f$ | $x_1$ | $x_2$ | $x_1$ | $x_2$ | $x_1$ | $x_2$ |
| 50 | Infeasible | | 12.02 | −10.08 | 12.02 | −10.09 |
| $10^2$ | Infeasible | | 12.02 | −10.09 | 12.02 | −10.09 |
| $10^3$ | 11.03 | −10.99 | 12.01 | −10.09 | 12.01 | −10.08 |
| $10^4$ | 11.39 | −10.98 | 12.01 | −10.09 | 12.01 | −10.08 |

## 6 | CONCLUSION

We have presented an optimization-based method for designing structured controllers minimizing the $\mathcal{H}_2$ or $\mathcal{H}_\infty$ norm of the closed-loop. The proposed approach is specifically designed to utilize a limited number of frequency points during synthesis, which distinguishes it from the bulk of other frequency-function-based methods. With careful overbounding, stability, and robust performance are guaranteed, even when considering only a finite number of frequencies and uncertainty in the dynamics of the process. Three examples are presented to demonstrate the applicability of the proposed method and highlight its advantages compared to similar methods.

## references

[1] Partington JR. Robust identification and interpolation in $\mathcal{H}_\infty$. International Journal of Control 1991;54(5):1281–1290.

[2] Gu G, Khargonekar P. Linear and nonlinear algorithms for identification in $\mathcal{H}_\infty$ with error bounds. IEEE transactions on automatic control 1992;37(7):953–963.

[3] Chen J, Nett CN, Fan MK. Worst-case system identification in $\mathcal{H}_\infty$: validation of apriori information, essentially optimal algorithms, and error bounds. In: 1992 American Control Conference IEEE; 1992. p. 251–257.

[4] Gu G, Khargonekar PP. A class of algorithms for identification in $\mathcal{H}_\infty$. Automatica 1992;28(2):299–312.

[5] Tu S, Boczar R, Packard A, Recht B. Non-asymptotic analysis of robust control from coarse-grained identification. arXiv preprint arXiv:170704791 2017;.

[6] Oymak S, Ozay N. Non-asymptotic identification of LTI systems from a single trajectory. In: 2019 American control conference (ACC) IEEE; 2019. p. 5655–5661.

[7] Sarkar T, Rakhlin A, Dahleh MA. Finite time LTI system identification. The Journal of Machine Learning Research 2021;22(1):1186–1246.

[8] Care A, Csáji BC, Campi MC, Weyer E. Finite-sample system identification: An overview and a new correlation method. IEEE Control Systems Letters 2017;2(1):61–66.

[9] Skogestad S, Postlethwaite I. Multivariable feedback control: analysis and design. john Wiley & sons; 2005.

[10] Den Hamer A, Weiland S, Steinbuch M. Model-free norm-based fixed structure controller synthesis. In: Proceedings of the 48h IEEE Conference on Decision and Control (CDC) held jointly with 2009 28th Chinese Control Conference IEEE; 2009. p. 4030–4035.

[11] van Solingen E, van Wingerden JW, Oomen T. Frequency-domain optimization of fixed-structure controllers. International Journal of Robust and Nonlinear Control 2018;28(12):3784–3805.

[12] Boyd S, Hast M, Åström KJ. MIMO PID tuning via iterated LMI restriction. Int J Robust Nonlinear Control 2016 May;26(8):1718–1731.

[13] Karimi A, Kammer C. A data-driven approach to robust control of multivariable systems by convex optimization. Automatica 2017 Nov;85:227–233.

[14] Bloemers T, Tóth R, Oomen T. Towards Data-Driven LPV Controller Synthesis Based on Frequency Response Functions. Proceedings of the IEEE Conference on Decision and Control 2019 12;2019-December:5680–5685.

[15] Daş E, Başlamışlı SÇ. Two degree of freedom robust data-driven fixed-order controller synthesis using convex optimization. ISA transactions 2021;114:291–305.

[16] Apkarian P, Noll D. Structured $\mathcal{H}_\infty$ control of infinite-dimensional systems. International Journal of Robust and Nonlinear Control 2018;28(9):3212–3238.

[17] Schuchert P, Karimi A. Frequency-domain data-driven position-dependent controller synthesis for Cartesian Robots. IEEE Transactions on Control Systems Technology 2023;.

[18] Markovsky I, Ossareh H. Finite-data nonparametric frequency response evaluation without leakage. Automatica 2024;159:111351.

[19] Pintelon R, Schoukens J. System identification: a frequency domain approach. John Wiley & Sons; 2012.

[20] Reinelt W, Garulli A, Ljung L. Comparing different approaches to model error modeling in robust identification. Automatica 2002;38(5):787–803.

[21] Oymak S, Ozay N. Revisiting ho–kalman-based system identification: Robustness and finite-sample analysis. IEEE Transactions on Automatic Control 2021;67(4):1914–1928.

[22] de Vries DK. Identification of Model Uncertainty for Control Design. Delft University of Technology; 1994.

[23] Marschner S, Shirley P. Fundamentals of computer graphics. CRC press; 2018.

[24] Boyd S, Boyd SP, Vandenberghe L. Convex Optimization. Cambridge university press; 2004.

[25] Löfberg J. YALMIP: A toolbox for modeling and optimization in MATLAB. In: 2004 International conference on robotics and automation IEEE; 2004. p. 284–289.

[26] Schuchert P, Karimi A. Achieving Optimal Performance With Data-Driven Frequency-Based Control Synthesis Methods. IEEE Control Systems Letters 2023;.

[27] Chen Y, Goulart P. An Efficient IPM Implementation for A Class of Nonsymmetric Cones. arXiv preprint arXiv:230512275 2023;.

[28] Galdos G, Karimi A, Longchamp R. Robust controller design by convex optimization based on finite frequency samples of spectral models. In: 49th IEEE Conference on Decision and Control (CDC) IEEE; 2010. p. 4317–4322.

# Appendices

## A | Derivation of bounding sets

The derivations of the sets $\mathscr{L}$ and $\mathscr{Q}$ are shown in this appendix for completeness. The focus is on first deriving a set $B$ such that $\Phi \in B$ which can be factored as

$$B = (1-\lambda)^2(p_0 + \Delta r_0) + 2(1-\lambda)\lambda(p_1 + \Delta r_1) + \lambda^2(p_2 + \Delta r_2),$$

Using as starting point (29):

$$\Phi \in \overline{Y} + \overline{P}\,\overline{X} + \Delta \cdot (\delta_Y + |\overline{P}|\delta_X + |\overline{X}|\delta_{\hat{P}} + \delta_X\delta_{\hat{P}})$$

the derivation will be split in two parts, between factors being multiplied by $\Delta$, and factors not being multiplied by $\Delta$. Expanding $\overline{Y}(\lambda) + \overline{P}(\lambda)\overline{X}(\lambda)$ results in

$$(1-\lambda)\,Y_k + \lambda\,Y_{k+1} + ((1-\lambda)\,\hat{P}_k + \lambda\,\hat{P}_{k+1})((1-\lambda)\,X_k + \lambda\,X_{k+1}),$$

and can be factored as

$$(1-\lambda)^2 \cdot (Y_k + \hat{P}_k X_k) + 2(1-\lambda)\lambda \cdot 0.5(Y_k + Y_{k+1} + \hat{P}_k X_{k+1} + \hat{P}_{k+1} X_k) + \lambda^2 \cdot (Y_{k+1} + \hat{P}_{k+1} X_{k+1})$$

and from this last expression, coefficients $p_0, p_1, p_2$ can be read off. Similarly, it is desired to factor the variable $\lambda$ in

$$\delta_Y + |\overline{P}|\delta_X + |\overline{X}|\delta_{\hat{P}} + \delta_X\delta_{\hat{P}} \tag{47}$$

which is multiplied by the uncertainty $\Delta$. This is not possible due to the absolute value in $|\overline{X}|$ and $|\overline{P}|$. Using the inequality,

$$|\overline{X}(\lambda)| \le (1-\lambda)\,|X_k| + \lambda\,|X_{k+1}|$$

as $0 \le \lambda \le 1$, and similarly for $|\overline{P}|$, (47) can be bounded by

$$\delta_Y + |\overline{P}|\delta_X + |\overline{X}|\delta_{\hat{P}} + \delta_X\delta_{\hat{P}} \le \delta_Y + ((1-\lambda)\,|\hat{P}_k| + \lambda\,|\hat{P}_{k+1}|)\delta_X + ((1-\lambda)\,|X_k| + \lambda\,|X_{k+1}|)\delta_{\hat{P}} + \delta_X\delta_{\hat{P}}.$$

The right-hand side of the last expression can be rearranged to result in

$$\begin{aligned}(1-\lambda)^2 \cdot (&\delta_Y + \delta_X\delta_{\hat{P}} + |X_k|\delta_{\hat{P}} + |\hat{P}_k|\delta_X) \\ &+ 2(1-\lambda)\lambda \cdot 0.5(2\delta_Y + 2\delta_X\delta_{\hat{P}} + \delta_{\hat{P}}(|X_k| + |X_{k+1}|) + \delta_X(|\hat{P}_k| + |\hat{P}_{k+1}|)) \\ &+ \lambda^2 \cdot (\delta_Y + \delta_X\delta_{\hat{P}} + \delta_X|\hat{P}_{k+1}| + \delta_{\hat{P}}|X_{k+1}|)\end{aligned}$$

from which coefficients $r_0, r_1, r_2$ can be read off. The set $B$ is not convex, but taking the convex hull of the control disks $p_i + \Delta r_i$ results in the desired set $\mathscr{L}$.

A similar derivation should be carried out to find a set $\mathscr{Q}$ such that

$$VY + WX \in \mathscr{Q}.$$

First, it is desired to find a Bézier curve such that

$$B' = (1-\lambda)^2 \cdot (q_0 + \mathbf{\Delta} s_0) + 2(1-\lambda)\lambda \cdot (q_1 + \mathbf{\Delta} s_1) + \lambda^2 \cdot (q_2 + \mathbf{\Delta} s_2)$$

and $VY + WX \in B'$. From definitions (20)–(23), a candidate set is

$$(\overline{V} + \mathbf{\Delta}\delta_V)(\overline{Y} + \Delta\delta_Y) + (\overline{W} + \mathbf{\Delta}\delta_W)(\overline{X} + \Delta\delta_X),$$

and can be rearranged using (28) as

$$\overline{V}\,\overline{Y} + \overline{W}\,\overline{X} + \mathbf{\Delta}(\delta_V|\overline{Y}| + |V|\delta_Y + \delta_V\delta_Y) + \mathbf{\Delta}(\delta_W|\overline{X}| + |W|\delta_X + \delta_W\delta_X). \tag{48}$$

Expanding $\overline{V}(\lambda)\,\overline{Y}(\lambda) + \overline{W}(\lambda)\,\overline{X}(\lambda)$ results in

$$((1-\lambda)\,V_k + \lambda\,V_{k+1})((1-\lambda)\,Y_k + \lambda\,Y_{k+1}) + ((1-\lambda)\,W_k + \lambda\,W_{k+1})((1-\lambda)\,X_k + \lambda\,X_{k+1})$$

and can be factored as

$$(1-\lambda)^2 \cdot (V_kY_k + W_kX_k) + 2(1-\lambda)\lambda \cdot 0.5(V_kY_{k+1} + V_{k+1}Y_k + W_kX_{k+1} + W_{k+1}X_k) + \lambda^2 \cdot (V_{k+1}Y_{k+1} + W_{k+1}X_{k+1})$$

and $q_0, q_1, q_2$ can be read of this last expression. Similarly, the factors on the first line of (48) being multiplied by $\mathbf{\Delta}$ can be bounded by

$$\delta_V|\overline{Y}| + |V|\delta_Y + \delta_V\delta_Y \preceq \delta_V((1-\lambda)\,|Y_k| + \lambda\,|Y_{k+1}|) + ((1-\lambda)\,|V_k| + \lambda\,|V_{k+1}|)\delta_Y + \delta_V\delta_Y,$$

where $\preceq$ indicates the element-wise inequality. The right-hand side can then be factored as

$$\begin{aligned}(1-\lambda)^2 \cdot (&\delta_V\delta_Y + \delta_V|Y_k| + \delta_Y|V_k|) \\ &+ 2(1-\lambda)\lambda \cdot 0.5(2\delta_V\delta_Y + \delta_V|Y_k| + \delta_Y|V_k| + \delta_V|Y_{k+1}| + \delta_Y|V_{k+1}|) \\ &+ \lambda^2 \cdot (\delta_V\delta_Y + \delta_V|Y_{k+1}| + \delta_Y|V_{k+1}|).\end{aligned} \tag{49}$$

Finally, the factors on the second line of (48) begin multiplied by $\mathbf{\Delta}$ can be bounded by

$$\delta_W|\overline{X}| + |W|\delta_X + \delta_W\delta_X \preceq \delta_W((1-\lambda)\,|X_k| + \lambda\,|X_{k+1}|) + ((1-\lambda)\,|W_k| + \lambda\,|W_{k+1}|)\delta_X + \delta_W\delta_X.$$

The right-hand side of this last expression can be factored as

$$\begin{aligned}(1-\lambda)^2 \cdot (\delta_W \delta_X + \delta_W |X_k| + \delta_X |W_k|) \\ + 2(1-\lambda)\lambda \cdot 0.5(2\delta_W \delta_X + \delta_W |X_k| + \delta_X |W_k| + \delta_W |X_{k+1}| + \delta_X |W_{k+1}|) \\ + \lambda^2 \cdot (\delta_W \delta_X + \delta_W |X_{k+1}| + \delta_X |W_{k+1}|),\end{aligned} \quad (50)$$

and $s_0, s_1, s_2$ can be identified from (49) and (50). The set $B'$ is not convex, but taking the convex hull of the control disks $q_i + \mathbf{\Delta} s_i$ results in the desired set $\mathscr{Q}$.

## B | Winding numbers

For a function in polar coordinates $f = r(t)e^{j\phi(t)}$, the argument not restricted to the interval $[-\pi, \pi)$ of this function is denoted $\arg\{f(t)\} = \phi(t)$. Given two regular closed-curves

$$C_1 : [0,1] \to \mathbb{C}/\{0\}, \quad C_2 : [0,1] \to \mathbb{C}/\{0\}$$

with respective polar representation

$$\begin{aligned}(r_1, \phi_1) : [0,1] \to \mathbb{R}_+ \times \mathbb{R} \\ (r_2, \phi_2) : [0,1] \to \mathbb{R}_+ \times \mathbb{R}\end{aligned}$$

such that $r_1, r_2, \phi_1, \phi_2$ are continuous functions on the unit interval, then

**Lemma 2** *if*

$$|\phi_1(t) - \phi_2(t)| \not\equiv \pi \mod 2\pi, \quad \forall t \in [0,1] \quad (51)$$

*then* $\text{wno}\{C_1\} = \text{wno}\{C_2\}$.

*Proof:* Without any loss of generality, assume that $\phi_1(0) = \phi_2(0) = 0$, then

$$|\phi_1(t) - \phi_2(t)| < \pi$$

since $\phi_1$ and $\phi_2$ continuous functions, and (51) prevent this difference from taking values equal to, and therefore larger than, $\pi$. The winding number (wno) of the two curves satisfies

$$\begin{aligned}\text{wno}\{C_1\} = \frac{1}{2\pi} \arg\{C_1(1)\} = \frac{1}{2\pi}\phi_1(1) \\ \text{wno}\{C_2\} = \frac{1}{2\pi} \arg\{C_2(1)\} = \frac{1}{2\pi}\phi_2(1)\end{aligned}$$

and the difference can be bounded by

$$|\operatorname{wno}\{C_1\} - \operatorname{wno}\{C_2\}| = \frac{1}{2\pi}|\phi_1(1) - \phi_2(1)| < \frac{\pi}{2\pi}$$

or equivalently

$$|\operatorname{wno}\{C_1\} - \operatorname{wno}\{C_2\}| < 0.5.$$

Since the winding number is an integer and, similarly, the difference between two winding numbers is also an integer, the only integer strictly smaller (in magnitude) than 0.5 is 0. Therefore, both curves have the same winding number, which concludes this proof. ■